Amyloid *β*-binding Bifunctional Chelators with Favorable Lipophilicity for ^{64}Cu PET Imaging in Alzheimer's Disease

Yujue Wang,[†] Truc T. Huynh,[‡,#] Hong-Jun Cho,[†] Yung-Ching Wang[†], Buck E. Rogers,[‡] and Liviu M. Mirica*[,†,§]

[†] Department of Chemistry, University of Illinois at Urbana-Champaign, 600 S. Mathews Avenue, Urbana, Illinois 61801, United States

[‡] Department of Radiation Oncology, Washington University School of Medicine, St. Louis, Missouri 63108, United States

[#] Department of Chemistry, Washington University, St. Louis, Missouri 63130, United States

§Hope Center for Neurological Disorders, Washington University School of Medicine, St. Louis, MO 63110, United States

KEYWORDS Alzheimer's disease, amyloid beta (Aβ) peptides, ^{64}Cu positron emission tomography (PET), bifunctional chelators, lipophilicity

ABSTRACT: Herein we report a new series of bifunctional chelators (BFCs) with high affinity for amyloid aggregates, strong binding affinity towards Cu(II) and favorable lipophilicity for potential blood-brain barrier (BBB) penetration. The alkyl carboxylate pendant arms offer up to three orders of magnitude higher binding affinity towards Cu(II) vs. the parent chelating fragment, and can generate fairly stable Cu complexes, including ^{64}Cu-radiolabeled compounds. Among the five compounds tested, the ^{64}Cu-YW-7 and ^{64}Cu-YW-10 complexes exhibit strong and specific staining of amyloid plaques in *ex vivo* autoradiography studies. Importantly, these compounds have promising partition coefficient (Log D) values of 0.91-1.26 and show moderate brain uptake in biodistribution studies using CD-1 mice. Overall, these BFCs could serve as lead compounds for the development of positron emission tomography (PET) imaging agents for AD diagnosis.

INTRODUCTION

Alzheimer's Disease (AD) is a progressive neurodegenerative disease and the most prevalent form of dementia. The progression of AD leads to synaptic failure and neuronal death, resulting in cognitive decline in memory, learning skill, and language.[1,2] The brains of AD patients are characterized by the deposition of senile plaques composed of the aggregates of amyloid β (Aβ). Aβ peptide is derived from the Aβ precursor protein (APP), and the main peptide alloforms are 42 and 40 amino acids long.[3-7]

To date, there is no cure for AD, the current treatments only alleviate the symptoms and are not able to modify the pathological progression of AD.[8] Early diagnosis of AD could contribute to a better preparation of intervention and care plan, making it possible for the maintenance of mild cognitive impairment and to improve the life quality. Molecular imaging modality such as positron emission tomography (PET) allows for non-invasive assessment of the Aβ burden in patients. Pittsburg compound B (^{11}C-PiB) is the most extensively studied amyloid PET imaging agent, but its clinical usage is greatly limited by short half-life (20 minutes) of ^{11}C.[9] In comparison, ^{18}F is a more suitable radioisotope with a longer half-life of 109.8 minutes. To date, three compounds have been approved by the US Food and Drug Administration (FDA) for amyloid imaging: the benzothiazole derivative ^{18}F-Flutemetamol (Vizamyl), the stilbene derivatives ^{18}F-Florbetaben (Neuraceq) and ^{18}F-Florbetapir (Amyvid).[10-13]

However, the relative short half-lives and the necessity of covalent incorporation of the ^{11}C and ^{18}F radionuclides have limited the widespread clinical usage of these imaging probes.[14] By comparison, the radionuclide ^{64}Cu has an optimal half-life of 12.7 hours, and its well established coordination chemistry allows for easy conjugation with the biologically relevant molecules.[15-17] Thus, ^{64}Cu PET imaging agents contain amyloid targeting fragments could assist in early diagnosis of AD and greatly facilitating the development of therapeutics for AD.[3,18-27]

For PET imaging purposes, a chelator that forms highly stable ^{64}Cu complexes is critical for minimizing off-target tissue uptake. 1,4,7-triazacyclononane (TACN) based ligands have been extensively studied as copper chelating agents, including radiotracers for molecular imaging.[28] Chelators that contain 1,4,7-triazacyclononane-1,4,7-triacetic acid (NOTA) ligands have shown stable ^{64}Cu-complexes formation *in vivo*. The acetic acid arms of the TACN backbone were proposed to enhance complexation with the metal ion by forming a hexadentate ligand that is known to form the ^{64}Cu complexes that are stable *in vitro* and *in vivo*.[29]

Nevertheless, the presence of several free carboxylic acid groups in these chelators limits the blood-brain barrier (BBB) permeability, which is usually the biggest limiting factor for imaging agents applied for the central nervous system (CNS).[30,31] Thus, herein we employ the strategy of using the ester derivative of the carboxylate pendant arm attached to the TACN backbone, in order to increase the lipophilicity of the bifunctional chelators (BFcs) and facilitate brain uptake. The additional O donor atoms from the ester arm lead to formation of metal complexes with greater stability *in vivo*. Inspired by the imaging probes mentioned above, our purpose is to design ester-based ^{64}Cu PET imaging agents that target the Aβ species and provide diagnostic information for AD.

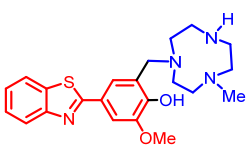

YW-6

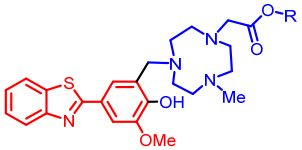

YW-7: R= $C(CH_3)_3$
YW-8: R= $CH(CH_3)_2$
YW-9: R= CH_2CH_3
YW-10: R= CH_3
YW-14: R=H

Figure 1. Structures of the ligands investigated herein. The metal-binding and Aβ-interacting fragments are shown in blue and red, respectively.

EXPERIMENTAL SECTION

General methods.

All reagents were purchased from commercial sources and used as received unless stated otherwise.1-methyl-1,4,7-triazacyclononane (MeH_2tacn) was synthesized according to reported procedures.[32] All solutions and buffers were prepared using metal-free Millipore water that was treated with Chelex overnight and filtered through a 0.22 μm nylon filter. ^{1}H (300 MHz) NMR spectra were recorded on a Varian Mercury-300 spectrometer or a VARIAN UNITY Inova 400 spectrometer. ^{13}C (126 MHz) NMR spectra were recorded on a VARIAN VXR 500 with UNITY INOVA Console spectrometer. Chemical shifts are reported in parts per million and referenced to residual solvent resonance peaks. UV−visible spectra were recorded on a Varian Cary 50 Bio spectrophotometer and are reported as λ_{max}, nm (ε, M^{-1} cm^{-1}). All fluorescence measurements were performed using a SpectraMax M2e plate reader (Molecular Devices). EPR spectra were recorded on a Bruker 10" EMXPlus X-band Continuous Wave EPR spectrometer at 77 K. EPR spectra simulation and analysis were performed using Bruker WINEPR SimFonia program, version 1.25. ESI-MS experiments were performed by the Mass Spectrometry Lab at UIUC using a Waters Q-TOF Ultima ESI mass spectrometer with an electron spray ionization source.

Synthesis of BFCs.

YW-7. To a suspension of YW-6 (100 mg, 0.24 mmol) and sodium carbonate (28 mg, 0.26 mmol) in MeCN (15 ml), tert-butyl bromoacetate (52 mg, 0.26 mmol) in MeCN (5 ml) was added. The reaction mixture was stirred at room temperature for 12 h. The solvent was removed to give an orange-yellow residue that was purified by Combi-Flash (reverse-phase) using MeCN/H_2O/TFA (40:60:0.1) to yield a yellow solution, which was then neutralized with $NaHCO_3$, extracted with dichloromethane and dried to give a yellow solid (118 mg, yield 93%).^{1}H NMR (400 MHz, $CDCl_3$) δ 7.98 (d, J = 8.1 Hz, 1H), 7.83 (d, J = 7.9 Hz, 1H), 7.56 (s, 1H), 7.48 – 7.38 (m, 2H), 7.32 (t, J = 8.1 Hz, 1H), 3.92 (d, J = 26.6 Hz, 5H), 3.25 (s, 6H), 2.98 (s, 4H), 2.82 (s, 3H), 2.68 (d, J = 21.8 Hz, 4H), 1.39 (s, 9H). ^{13}C NMR (126 MHz, $CDCl_3$) δ 171.49, 168.34, 154.39, 148.54, 135.00, 126.48, 125.03, 123.87, 122.93, 121.73, 110.06, 56.55, 29.95, 28.41. HR-ESI-MS: Calcd for $[M+H]^+$, 527.2647; Found, 527.2680.

YW-8. To a suspension of YW-6 (20 mg, 0.05 mmol) and sodium carbonate (6 mg, 0.05 mmol) in MeCN (5 ml), iso-propyl bromoacetate (10 mg, 0.05 mmol) in MeCN (5 ml) was added. The reaction mixture was stirred at room temperature for 24 h. The solvent was removed to give a yellow residue that was purified by Combi-Flash (reverse-phase) using MeCN/H_2O/TFA (45:55:0.1) to yield a yellow solution, which was then neutralized with $NaHCO_3$, extracted with dichloromethane and dried to give a yellow solid (16 mg, yield 64%). ^{1}H NMR (300 MHz, $CDCl_3$) δ 8.01 (d, J = 9.3 Hz, 1H), 7.87 (d, J = 9.2 Hz, 1H), 7.61 (s, 1H), 7.53 – 7.42 (m, 2H), 7.41 – 7.31 (m, 1H), 4.98 (p, J = 6.2 Hz, 1H), 4.02 (s, 5H), 3.39 (s, 4H), 3.06 (s, 4H), 2.90 (s, 3H), 2.73 (s, 4H), 1.21 (d, J = 6.3 Hz, 5H). ^{13}C NMR (126 MHz, $CDCl_3$) δ 171.91, 168.53, 134.97, 126.44, 124.95, 123.53, 122.88, 121.71, 110.01, 68.29, 58.41, 57.27, 56.48, 29.95, 22.18. HR-ESI-MS: Calcd for $[M+H]^+$, 513.2491; Found, 513.3100.

YW-9. To a suspension of YW-6 (36 mg, 0.09 mmol) and sodium carbonate (9 mg, 0.09 mmol) in MeCN (10 ml), ethyl bromoacetate (52 mg, 0.26 mmol) in MeCN (5 ml) was added. The reaction mixture was stirred at room temperature for 12 h. The solvent was removed to give an orange-yellow residue that was purified by Combi-Flash (reverse-phase) using MeCN/H_2O/TFA (50:50:0.1) to yield a yellow solution, which was then neutralized with $NaHCO_3$, extracted with dichloromethane and dried to give a yellow solid (14 mg, yield 33%). ^{1}H NMR (300 MHz, $CDCl_3$) δ 8.00 (d, J = 8.6 Hz, 1H), 7.86 (d, J = 8.6 Hz, 1H), 7.57 (s, 1H), 7.50 – 7.42 (m, 1H), 7.40 (d, J = 2.0 Hz, 1H), 7.37 – 7.30 (m, 1H), 4.12 (q, J = 7.1 Hz, 2H), 4.00 (s, 3H), 3.92 (s, 2H), 3.13 – 2.73 (m, 12H), 2.66 (s, 3H), 1.38 – 1.14 (m, 6H). ^{13}C NMR (126 MHz, $CDCl_3$) δ 172.17, 154.38, 148.61, 134.99, 130.50, 127.29, 126.47, 125.02, 122.91, 121.73, 110.10, 63.04, 60.75, 60.21, 56.53, 52.95, 29.95, 14.48. HR-ESI-MS: Calcd for $[M+H]^+$, 499.2334; Found, 499.2919.

YW-10. To a suspension of YW-6 (25 mg, 0.06 mmol) and sodium carbonate (28 mg, 0.26 mmol) in MeCN (15 ml), tert-butyl bromoacetate (52 mg, 0.26 mmol) in MeCN (5 ml) was added. The reaction mixture was stirred at room temperature for 16 h. The solvent was removed to give an orange-yellow residue that was purified by Combi-Flash (reverse-phase) using MeCN/H_2O/TFA (45:55:0.1) to yield a yellow solution, which was then neutralized with $NaHCO_3$, extracted with dichloromethane and dried to give a yellow solid (15 mg, yield 51%).^{1}H NMR (300 MHz, $CDCl_3$) δ 8.00 (d, J = 9.2 Hz, 1H), 7.86 (d, J = 8.5 Hz, 1H), 7.57 (s, 1H), 7.51 – 7.41 (m, 1H), 7.35 (dd, J = 16.8, 8.3 Hz, 2H), 3.99 (s, 3H), 3.92 (s, 2H), 3.66 (s, 3H), 3.11 – 2.73 (m, 12H), 2.64 (s, 3H). ^{13}C NMR (126 MHz, $CDCl_3$) δ 172.95, 168.72, 151.65, 148.8, 126.38, 124.84, 122.84, 121.68, 120.88, 110.03, 60.78, 58.47, 56.43, 55.87, 53.68, 46.68, 29.95. HR-ESI-MS: Calcd for $[M+H]^+$, 485.2178; Found, 485.2794.

YW-14. The ester YW-7 (50 mg, 95 mmol) was dissolved in 10 mL of 6 M HCl and stirred at room temperature for 24 h. The solvent was removed to get a yellow residue, which was dissolved in diethyl ether and filtered. Removal of the solvent gave a light-yellow powder, which was dried under vacuum to obtain the product (11 mg, yield 25%). ^{1}H NMR (499 MHz, CD_3OD) δ 8.47 (s, 1H), 8.13 (dd, J = 29.6, 8.1 Hz, 2H), 7.97 (s, 1H), 7.67 (dt, J = 48.7, 7.3 Hz, 2H), 4.09 (s, 4H), 4.01 (s, 2H), 3.63 – 3.29 (m, 12H), 3.08 (s, 3H). ^{13}C NMR (126 MHz, CD_3OD) δ 172.59, 153.19, 149.21, 129.33, 127.82, 123.47, 111.71, 56.65, 54.76, 50.68. HR-ESI-MS: Calcd for $[M+H]^+$, 471.2021; Found, 471.2058.

Acidity and Stability Constants Determination. UV-Vis pH titrations were employed for the determination of acidity constants of BFCs and stability constants with Cu(II). For acidity constants, solutions of ligands **YW-6** to **YW-10** (20 μM, 0.1 M NaCl, pH 3) were titrated with small aliquots of 0.1 M NaOH, and **YW-14** (20 μM, 0.1 M NaCl, pH 1.2) was titrated with small aliquots of 1 M NaOH at room temperature under a steady moist flow of N_2. At least 30 UV-vis spectra were collected in the pH 1.2-11 range. DMSO stocks (10 mM) were diluted in MeOH-water mixture in which MeOH did not exceed 1% (v:v). Similarly, stability constants were determined by titrating solutions of **YW-7** to **YW-10** and 0.9 equivalent of $Cu(ClO_4)_2.6H_2O$

(18 μM) with small aliquots of 0.2 M NaOH at room temperature. Solution of **YW-14** and 0.9 equivalent of $Cu(ClO_4)_2.6H_2O$ (18 μM) was titrated with small aliquots of 1 M NaOH. At least 30 UV-vis spectra were collected in the pH 1.2-11 range. The acidity and stability constants were calculated using the HypSpec computer program (Protonic Software, UK).[33] Speciation plots of the compounds and their metal complexes were calculated using the program HySS2009 (Protonic Software, UK).[34]

Histological Staining of 5xFAD Mouse Brain Sections. Eleven-month-old 5xFAD mouse brain sections were blocked with bovine serum albumin (2% BSA in PBS, pH 7.4, 10 min) and covered with a PBS solution of BFC for 30 min, then with Congo Red (2 μM) solution for 30 min. The sections were treated with BSA again (4 min) to remove any compound non-specifically bound to the tissue. Finally, the sections were washed with PBS (3 × 2 min), DI water (2 min), and mounted with non-fluorescent mounting media. For antibody staining, six-month-old 5xFAD mouse brain sections were incubated with the AF594-conjugated anti-Aβ antibody (AF594-HJ3.4 antibody)[35,36] solution (1 μg/ml) at room temperature for 1 h. The stained brain sections were imaged using a Zeiss LSM 7010 confocal fluorescent microscope and Invitrogen EVOS FL Auto 2 Imaging System (Thermo Fisher, USA).

Job's plots for solution stoichiometry determination. To determine the ligand:Cu stoichiometry for BFC, a stock solution (500 μM) of and $CuCl_2 \cdot H_2O$ (500 μM) were prepared in DMSO and spectra were measured using a Cary Bio UV-Vis instrument. Each ligand has the same metal binding motif, therefore each ligand is assumed to bind to Cu(II) in a similar manner. Solutions containing different ratios of ligand and Cu ions were recorded from 0 to 100 mol % Cu (total concentration = 25 μM). Appropriate amounts of the stock solutions were dissolved into 500 μL of PBS pH 7.4 buffer and allowed to equilibrate for 5 minutes before recording the spectra.

Radiolabeling. ^{64}Cu was produced by a (p,n) reaction on enriched ^{64}Ni on a CS-15 biomedical cyclotron (Cyclotron Corporation, Berkeley, CA) at Mallinckrodt Institute of Radiology, Washington University School of Medicine, and purified with an automated system using standard procedures.[37,38] The BFCs were stored as DMSO stocks. The compounds were diluted to get a concentration of 1 mM. 20 μL of the BFC solution was added to 100 μL of 0.1 M NH_4OAc (pH 5.5), following by the addition of 7.4 MBq (200 μCi) of ^{64}Cu stock solution. Various conditions (temperatures, pH and reaction times) were attempted to optimize the labeling efficiency. For **YW-7**, **YW-10,** and **YW-14**, the reaction mixture was incubated at 45 °C for 1 h. For **YW-8** and **YW-9**, the mixture was incubated at 80 °C for 2 h. Radiolabeled compounds were analyzed by HPLC, with water (0.1% TFA) and acetonitrile (0.1% TFA) as the mobile phases and with a gradient of 0–100% acetonitrile over 12 minutes with a flow rate of 1 mL/min. No further purification was needed if ^{64}Cu-labeled complexes were obtained in high radiochemical yield (>95%).

Lipophilicity Studies. Ten replicate Eppendorf tubes of 1:1 (v/v) n-octanol and PBS 1X were prepared (500 μL each). The ^{64}Cu-labeled complexes (0.37 MBq, 10 μCi) were added to each tube, vortexed and incubated on a thermomixer with 1000 rpm for 1 h. After 1 h, the solution was kept without shaking for 30 minutes to allow for the separation of the two layers. Aliquots (100 μL) from the aqueous and the n-octanol layers were removed and counted separately in an automated gamma counter. The partition coefficients were calculated using the ratio of (activity detected in n-octanol)/(activity detected in aqueous layer) to get the *log* D_{oct} values. The overall average was recorded as the final *log* D_{oct} value for each compound. High *log* D_{oct} (1-2.5) is desired as it indicates the ability of labeled products in crossing the BBB and reaching therapeutic concentrations in the brain.

Biodistribution Studies. All animal experiments were performed in compliance with the Guidelines for Care and Use of Research Animals established by the Division of Comparative Medicine and the Animal Studies Committee of Washington University School of Medicine. Initial biodistribution studies were conducted in wild type CD-1 female mice (Charles River Laboratories) of age 5-7 weeks. The injection dose was prepared by diluting into a 90 % saline solution. The mice were injected via the tail vein with 0.22-0.37 MBq (6-10 μCi) of each compound per animal in 100 μL saline solution. After each time point (2, 60, and 240 min), mice were anesthetized with 1 - 2 % isoflurane and euthanized by cervical dislocation Brain, blood, kidney, liver and other organs of interest were harvested and amount of radioactivity in each organ was counted on a gamma counter containing a NaI crystal. The data were corrected for radioactive decay and percent injected dose per gram (%ID/g) of tissue was calculated. All samples were calibrated against a known standard. Quantitative data were processed by Prism 8 (GraphPad Software, v 6.03, La Jolla, CA) and expressed as Mean ± SD. Statistical analysis performed using one-way analysis of variance and Student's t test. Differences at the 95% confidence level ($p < 0.05$) were considered statistically significant.

***Ex vivo* Autoradiography Studies.** Brain sections of 11-month-old 5xFAD transgenic mice and aged-matched WT mice were obtained as described previously and immersed into a cryo-protectant solution. These sections were sorted and carefully removed using phosphate buffer in saline (PBS) to a 12-well plate. Each section was washed with 100% PBS three times, and ~0.925 MBq (25 μCi) of ^{64}Cu-labeled BFC in 2.5 mL PBS was added to completely cover the brain section and incubate for 1 h at room temperature in a shielded bunker. Blocking solution using blocking agent was added to evaluate the specific binding of radiolabeled compounds.[39] After the incubation, brain sections (WT, 5xFAD, 5xFAD with blocking) were washed using 1:1 (v/v) ethanol and PBS twice and PBS once for 10 minutes of each washing cycle. Brain sections were removed, mounted onto microscopic slides and briefly air-dried. The imaging slides were then mounted onto phosphor imaging screen plate (GE Healthcare Life Sciences), and were exposed overnight in -20 °C. The plates were scanned using a phosphor imager plate scanner (Storm 840) and the resulting images were processed using ImageJ (v1.48, public domain) software.

RESULTS AND DISCUSSION

Design and syntheses of Bifunctional Chelators. The Bifunctional chelators (BFCs) discussed herein are constructed by linking the Aβ-binding 2-phenyl-benzothiazole and o-vanillin fragments with the metal-chelating TACN ligand via Mannich reaction with paraformaldehyde (Scheme 1). The amyloid targeting motif was generated by the condensation of 2-aminothiophenyl with vanillin, followed by oxidation with atmospheric

oxygen (Scheme S1). This heterocyclic fragment is derived from Thioflavin T (ThT), a well-known amyloid-binding fluorescent dye that shows high binding affinity toward Aβ species,[40] and that has been utilized as the amyloid targeting motif in multifunctional compounds for PET imaging and treatment of AD.[20-22,41-43]

To further enhance the metal chelation ability of BFCs, the pendant carboxylate arms were added to the TACN backbone by reacting **YW-6** with a series of alkyl-bromoacetates, generating final products **YW-7** to **YW-10** that contain tert-butyl, iso-propyl, ethyl, and methyl ester groups, respectively. Hydrolysis of **YW-7** in presence of concentrated hydrochloric acid generates **YW-14**, which is a carboxylic acid and has the lowest molecular weight (<500 Da) among the BFCs, which is a factor for penetration of BBB according to Lipinski's rules.[44]

Absorption spectra were acquired to determine the maximum UV-Vis absorbance wavelength (λ_{abs}) of the ligands and their Cu(II) complexes in PBS (pH=7.4) buffer (Figure S1, S2). Based on the UV-Vis absorbance spectra, excitation wavelengths (λ_{ex}) of 328-332 nm (for ligands) and 349 nm (for Cu(II) complexes) were used to examine the fluorescent properties (Figure S3, S4). Results indicate a ~20 nm Stokes shift upon chelation with Cu(II), and the fluorescence intensity decreased due to quenching effect by Cu(II).

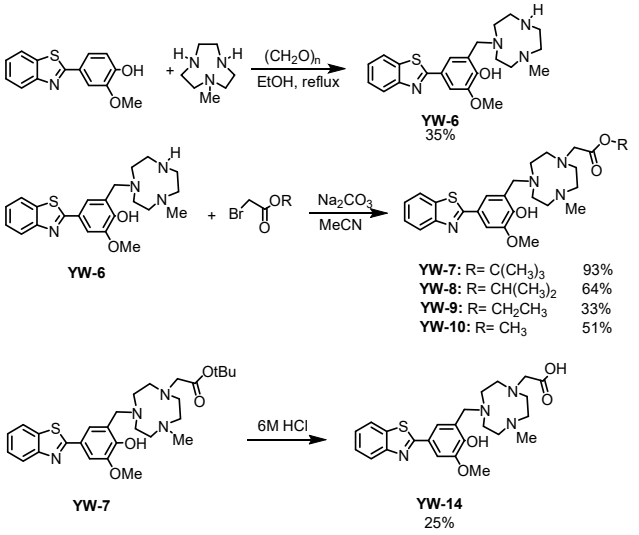

Scheme 1: Syntheses of BFCs.

Fluorescence Imaging of Amyloid Plaques in 5xFAD Mouse Brain Sections. *Ex vivo* mouse brain section staining was performed to evaluate each BFC's affinity toward Aβ species. Brain sections were collected from 11-month-old 5xFAD mice. An appreciable amount of fluorescence staining was observed upon incubation of the brain sections for 30 min with 50 μM solutions of our BFCs (Figures 2, left panel). The specific staining of amyloid plaques was confirmed by staining with Congo Red, another commonly used amyloid-binding fluorescent dye (Figure 2, middle panel). The fluorescent properties of BFCs indicate they exhibit labeling signal in the DAPI channel, which does not interfere with the Congo Red signal in the Texas Red channel. The labeling ability of Cu(II) complexes was also probed using same age mouse brain sections. Compared with BFCs, the colocalization of Cu(II) complexes signal with Congo Red signal is improved as indicated by Pearson's coefficients, especially for **YW-7**, **YW-10**, and **YW-14** (Figure 3). Other BFCs and their Cu(II) complexes also show moderate staining of amyloid aggregates (Figure S20). Overall, these *ex vivo* amyloid binding studies suggest that these BFCs show specific binding toward Aβ species (see below).

Ligand	Conc. (μM)	Ligand to Congo Red ratio
YW-7	50	25:1
YW-10	50	25:1
YW-14	50	25:1

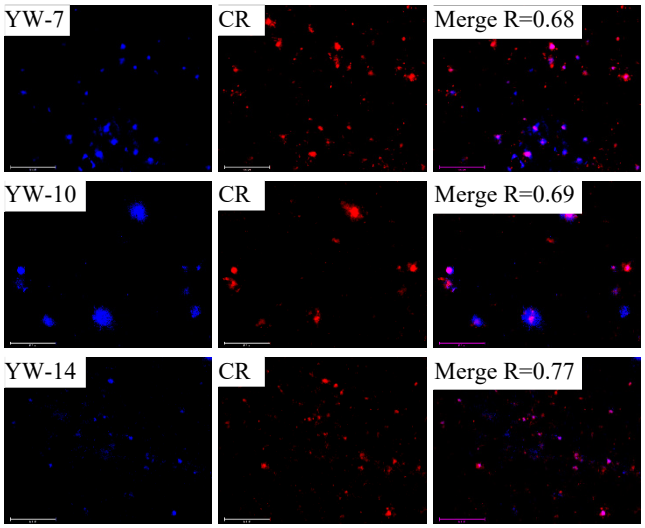

Figure 2. Fluorescence microscopy images of 5xFAD brain sections incubated with compounds **YW-7, YW-10,** and **YW-14** (left panels), Congo Red (middle panels), and merged images (right panels). Magnification: 20x. Scale bar: 125 μm.

Cu(II) complex	Conc. (μM)	Complex to CR ratio
Cu-YW-7	50	25:1
Cu-YW-10	50	25:1
Cu-YW-14	50	25:1

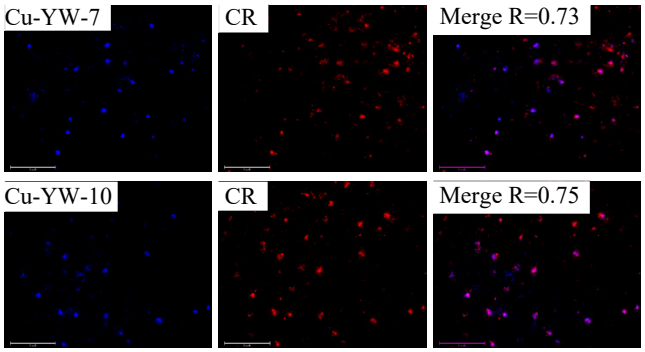

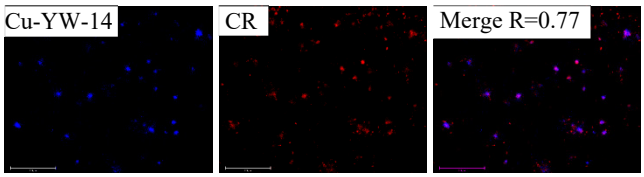

Figure 3. Fluorescence microscopy images of 5xFAD brain sections incubated with Cu(II) complexes of **YW-7, YW-10,** and **YW-14** (left panels), Congo Red (middle panels), and merged images (right panels). Magnification: 20x. Scale bar: 125 µm.

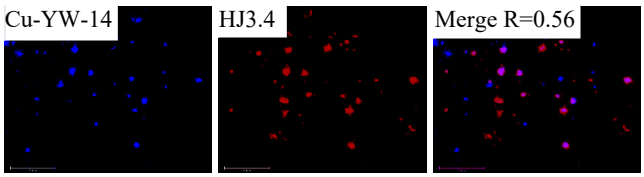

Figure 4. Fluorescence microscopy images of 5xFAD brain sections incubated with **YW-7, YW-10,** and **YW-14** as well as their Cu(II) complexes (left panels), AF594-HJ3.4 (middle panels), and merged images (right panels). Magnification: 20x. Scale bar: 125 µm.

Fluorescent dye labeled HJ3.4 antibody was utilized to confirm BFCs and their Cu(II) complexes' specific staining of Aβ plaques (Figure 4). This AF594-conjugated HJ3.4 antibody (AF594-HJ3.4) has shown binding to a range of Aβ species in previous published results.[22,35,36,45-47] In this study, younger mouse brain sections (6-month-old) were used to evaluate BFCs binding affinities, a heavy load of Aβ plaques signal was observed upon treatment with conditions described in the experimental section. AF594-HJ3.4 antibody exhibits larger staining spots for the amyloid aggregates compared with Congo red, our compounds and corresponding Cu(II) complexes still show favorable colocalization with antibody signals as suggested by the calculated Pearson's coefficients (Figure 4).

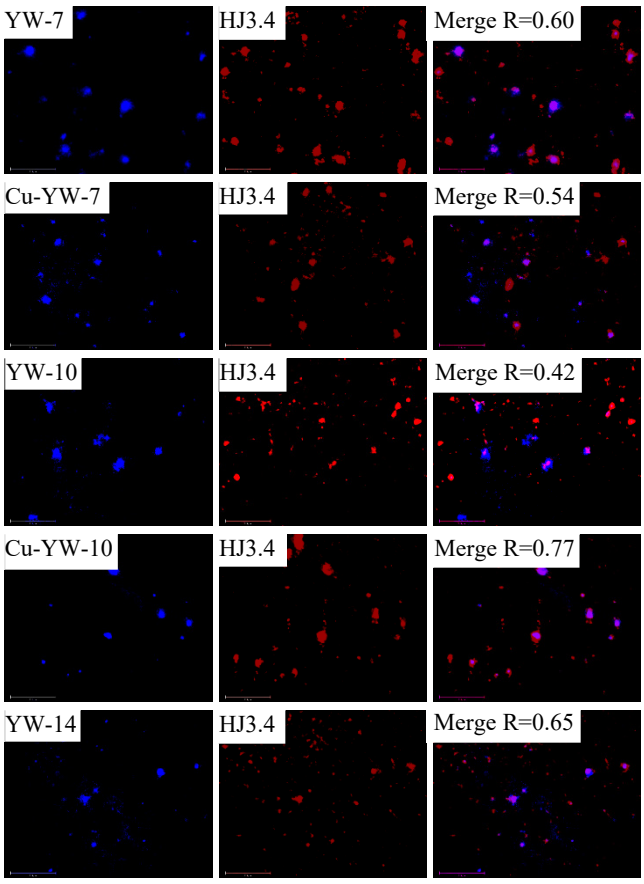

Acidity Constants of BFCs and Stability Constants of Cu(II) Complexes. Since all BFCs contain several acidic and basic functional groups, their acidity constants (pKa, log of the acid ionization constant) were determined by UV-Vis spectrophotometric titrations. For **YW-7**, UV-Vis titrations from pH 2.8 to 11.0 reveal several changes in the spectrum (Figure 5a), such as the disappearance of the band at 325 nm and the increase of the band at 367 nm with an isosbestic point at 341 nm. The best fit to the data was obtained with four pKa values: 3.09(8), 6.23(6), 8.08(3) and 8.81(1) (Table 1). Based on previously reported acidity constants for phenols and amines,[20,43] we assigned the three lower pKa values to the deprotonation of the amine groups of TACN backbone, and the highest pKa value to the phenol deprotonation in ligand. Ester containing-ligands in the series show similar values to those obtained for **YW-7** (Table 1).

YW-14, which contains the carboxylic acid instead of ester, was probed from pH 1.75 to 11.0 and the best fit was obtained with five pKa values: 1.37(1), 4.53(1), 6.18(8), 8.43(7) and 9.87(3). (Table S1). The lowest pKa value can be assigned to the deprotonation of the carboxylic acid group.

(a)

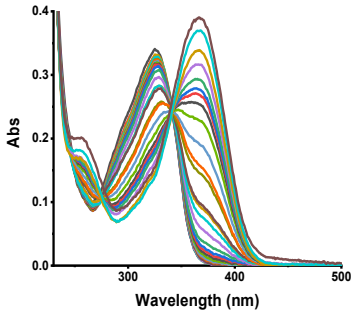

(b)

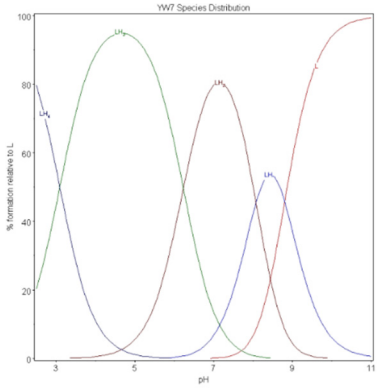

Figure 5. (a)Variable pH (pH 2.8−11.0) UV-Vis spectra of **YW-7** ([L] = 20 μM, 25 °C, I = 0.1 M NaCl) and (b) species distribution plot.

Table 1. Acidity constants (pK_a's) of **YW-6** to **YW-10** determined by spectrophotometric titrations (errors are for the last digit).

Reaction	YW-6	YW-7	YW-8	YW-9	YW-10
$[H_4L]^{3+} = [H_3L]^{2+} + H^+$ (pK_{a1})	4.15(5)	3.09(8)	3.14(5)	2.60(5)	3.40(1)
$[H_3L]^{2+} = [H_2L]^{+} + H^+$ (pK_{a2})	6.60(4)	6.23(6)	5.49(5)	5.00(3)	6.26(9)
$[H_2L]^{+} = [HL] + H^+$ (pK_{a3})	7.93(3)	8.08(3)	8.50(4)	8.30(2)	8.32(8)
$[HL] = [L]^{-} + H^+$ (pK_{a4})	9.90(1)	8.81(1)	10.19(2)	9.49(1)	10.43(4)

Table 2. Stability constants (logK) of the Cu(II) complexes of **YW-6** to **YW-14**.

Reaction	YW-6	YW-7	YW-8	YW-9	YW-10	YW-14
$M^{2+} + HL = [MHL]^{2+}$	6.60(1)	5.24(8)	4.55(4)	5.26(2)	4.59(2)	4.55(2)
$M^{2+} + L^{-1} = [ML]^{+}$	16.10(1)	19.50(4)	18.47(2)	18.88(2)	17.36(1)	20.92(1)

In order to quantify the metal chelation ability of the BFCs, we performed spectrophotometric titrations of ligands in presence of Cu(II) ion. To ensure full chelation of the ligand with Cu(II), 0.9 equivalent of $Cu(ClO_4)_2.6H_2O$ was added. As shown in Figure 6a the band at 325 nm disappears and the band at 352 nm rises when pH value increases, generating an isosbestic point at 333 nm. The pK_a's values of the ligands and the deprotonation of metal-bound water molecules were included in the calculation.

The calculated stability constants shown in Table 2 indicate that the Cu(II) complex of **YW-7** exhibits a stability constant that is ~3 orders of magnitude larger than that of **Cu-YW-6** (Table 2), which is expected given the presence of an additional metal-chelating acetate arm. In addition, **Cu-YW-7** has the highest log K value (~19.5) among the four different alkyl ester arm BFCs. Interestingly, the log K value of **Cu-YW-7** is only ca. one order of magnitude lower that the log K value of ~20.9 for **Cu-YW14**, suggesting that having a BFC with an ester arm instead of a carboxylic acid arm does not dramatically lower the stability constant for the corresponding Cu(II) complex. This is important for our . The steric hindrance of bulky tert-butyl group could be affecting the chelation of acetate arm to Cu(II) center.

Species distribution plot of **YW-7** and Cu(II) system was obtained based on the calculated stability constants (Figure 6b), and the concentration of free Cu^{2+} with **YW-7** is negligible above pH 4.5, the main species at physiological condition is **Cu-YW-7**. The concentrations of unchelated Cu^{2+} (pM =−log[$M_{unchelated}$]) at a specific pH value and total ion concentration can be calculated from the solution speciation diagrams (Table 3). These pM values could be used as a direct estimate of the ligand-metal affinity and a comparison for metal affinity among difference ligands.[43,48,49] In this work, the calculated pCu values for **YW-7** and **YW-14** are both 10.8 at pH 7.4, comparable to that of the strong chelating agent DTPA (diethylenetriaminepentaacetic acid), which is 10.7 at pH 7.4, indicating that our BFCs have high Cu(II) binding affinity.

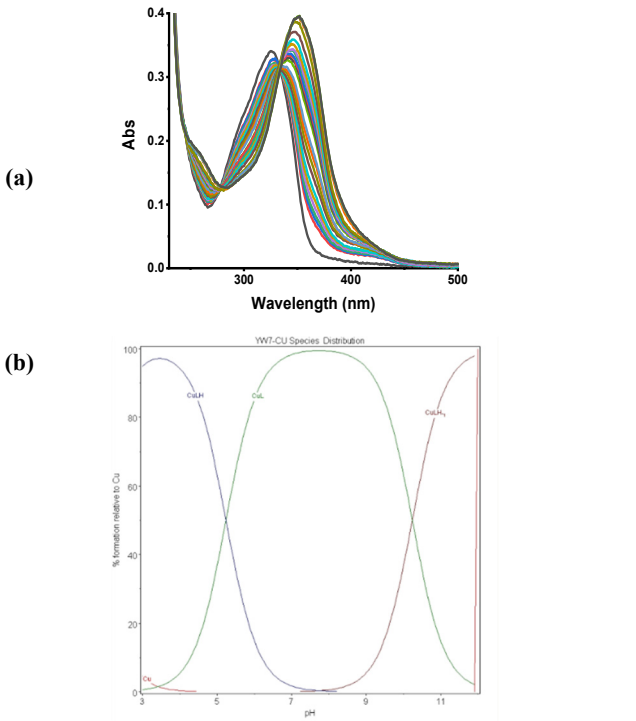

Figure 6. (a) Variable pH (pH 3−11) UV-Vis spectra of **YW-7** and Cu(II) system ([L] = 20 μM, $[Cu^{2+}]$ = 18 μM, 25 °C, I = 0.1 M NaCl) and (b) species distribution plot.

Table 3. Calculated pM ($-\log[M]_{free}$; M = Cu^{2+}) values for a solution containing a 1:1 Metal/Ligand Mixture ($[M^{2+}]_{tot}$ = [Ligand]$_{tot}$ = 50 μM)

	YW6	YW7	YW8	YW9	YW10	YW14	DTPA[a]
pH 6.6	7.8	10.0	8.6	9.3	8.2	9.9	9.7
pH 7.4	8.7	10.8	9.5	10.1	9.4	10.8	10.7

[a]Diethylenetriaminepentaacetic acid (DTPA), ref 43.

EPR spectra of Cu(II) complexes. To further characterize the Cu(II) complexes of BFCs, their X-band EPR spectra were recorded in frozen glasses at 77 K. The Cu(II) complexes were prepared right before the EPR experiment by reacting the BFC with 0.8 equivalent of $CuCl_2$. The EPR spectrum of the **Cu-YW-7** in a 1:1 (v/v) PBS/glycerol glass solution reveals a pseudoaxial EPR pattern with three different g values: g_x = 2.252, g_y = 2.05, and g_z = 2.00, A_x (Cu)=180G (Figure 7). The EPR spectrum of **Cu-YW-14** was also obtained in the same way and exhibits a similar EPR pattern as **YW-7**'s with g_x = 2.240, g_y = 2.085, and g_z = 2.030, A_x (Cu)=168G (Figure S22).

A different solvent system was also applied to study the Cu(II) complexes in a non-aqueous environment using 1:3 (v/v) acetonitrile/butyronitrile glass solution, and both complexes show similar patterns to those in aqueous solution (Figure S23, S24). EPR spectra of Cu(II) complexes of **YW-8, YW-9,** and **YW-10** were also collected in 1:3 (v/v) acetonitrile/butyronitrile glass solution (Figure S25, S26, S27).

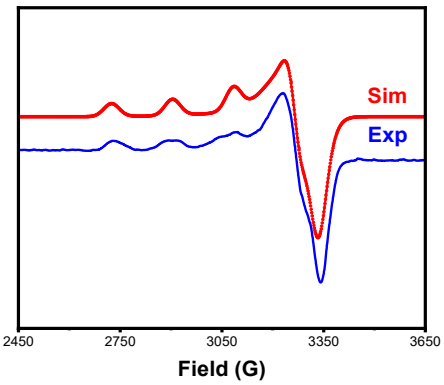

Figure 7. Experimental and Simulated EPR spectra of the **Cu-YW-7** complex in a 1:1 PBS/glycerol glass at 77 K. The following parameters were used for the simulation: g_z = 2.252, g_y = 2.075, and g_x = 2.045, A_x (Cu)= 165 G.

Radiolabeling and *Log D_{oct}* value determination. The radiolabeling of compounds **YW-7** to **YW-14** was performed using $^{64}CuCl_2$ and employing the conditions described in the experimental section. The novel chelators were readily labeled with ^{64}Cu under mild conditions. Quality control assays were conducted using HPLC and/or TLC, and HPLC retention times were observed in the range of 9.1~9.5 minutes for the ^{64}Cu-radiolabeled complexes (Figures S28). All radiochemical purities were >95% within minutes at 45 °C, with specific activities of 100 Ci/mmol or greater. Therefore, all radiolabeled complexes were used directly without further purification.

One important aspect of developing an imaging agent for AD is that it should be able to effectively cross the BBB. To determine the hydrophobicity of the radiolabeled compounds, the octanol/PBS partition coefficient values *log D_{oct}* were determined for the ^{64}Cu complexes of **YW-7** to **YW-14** (Table 4). The decreasing of esters' *log D_{oct}* values was observed with less bulky alkyl groups. Gratifyingly, the obtained *log D_{oct}* values for the ^{64}Cu-radiolabeled complexes **YW-7** to **YW-10** are in the range of 0.91 – 1.26, which suggests their potential ability to cross the BBB.[50] Interestingly, the ^{64}Cu complex of **YW-14**, which does not contain the alkyl ester group, has a positive *log D_{oct}* value of 1.15 ± 0.02 and is very likely to cross the BBB. The carboxylic acid group is normally not favorable for molecules designed to pass BBB due to its hydrophilicity and hydrogen bond forming property. We propose the chelation of carboxylic acid group in **YW-14** with the Cu(II) center generates a neutral complex and therefore is beneficial for BBB penetration. We are aware that compounds with slightly higher *log D_{oct}* values (ideally larger than 1) would be desirable, thus we chose **YW-7, YW-8, YW-9, YW-10, and YW-14** for the further characterization including autoradiography and biodistribution studies.

Table 4. Properties of ligands **YW-7 to YW-14**, measured *log D_{oct}* values for the corresponding ^{64}Cu-radiolabeled complexes.

Ligand	Molecular Weights (g·mol^{-1})	*log D_{oct}*
YW-7	527.0	1.26 ± 0.02
YW-8	512.7	1.07 ± 0.05
YW-9	498.6	1.01 ± 0.05
YW-10	484.6	0.91 ± 0.02
YW-14	470.6	1.15 ± 0.02

Autoradiography studies. *Ex vivo* autoradiography studies using brain sections of 5xFAD mice were conducted to determine the specific binding of the ^{64}Cu-labeled BFCs to the amyloid plaques. The brain sections were stained, washed, and imaged as described in the experimental section. By comparing with the wild type (WT) brain sections that show a limited background intensity (Figure 8, first row), an increased autoradiography intensity was observed upon treatment of the 5xFAD mouse brain sections with the ^{64}Cu-labeled complexes of **YW-7** to **YW-14** (Figure 8, third row). The specific binding to amyloid plaques of the radiolabeled BFC was further confirmed by blocking the brain sections with the non-radioactive blocking agent B_1 (Figure S29), which led to a remarkable decreased autoradiography intensity (Figure 8, second row). Except for **YW-7** that exhibits a slight degree of non-specific binding, the other BFCs all showed a significantly more intense signal for the 5xFAD mouse sections than the WT mouse sections. The ratios of average radioactivity of transgenic sections over WT sections are shown in Figure 9. Notably, **^{64}Cu-YW-10** exhibits a 7.5 intensity ratio of AD mouse section staining to WT sections. Due to the low signal intensity of **^{64}Cu-YW-14**, more radioactivity (35 μCi) was applied in additional experiments and the difference between WT sections and AD sections is more obvious (Figure S30), although **^{64}Cu-YW-14** exhibits the least specific amyloid-binding ability among all BFCs, likely due to the likely cationic nature of this complex. Overall, these autoradiography results strongly suggest that the ^{64}Cu-labeled BFCs **YW-7** to **YW-14** exhibit the ability to detect Aβ species *ex vivo*.

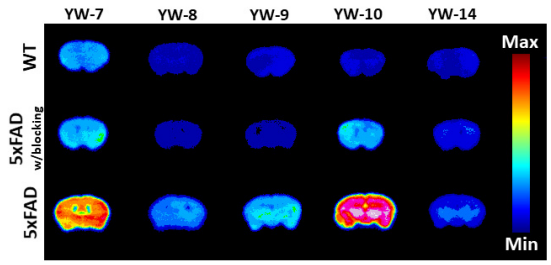

Figure 8. Autoradiography images of brain sections of WT and 5xFAD mice, in the absence and presence with a known Aβ specific blocking agent.

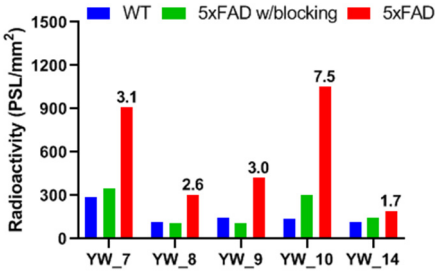

Figure 9. Average radioactivity of the brain sections in the autoradiography images. The numbers in the bar graph are the intensity ratios of 5xFAD to WT in each group.

Biodistribution Studies. Encouraged by the promising *in vitro* results, *in vivo* biodistribution experiments were then performed to investigate the pharmacokinetics of **^{64}Cu-YW-7** to **^{64}Cu-YW-14** complexes using CD-1 mice. The retention and accumulation of the ^{64}Cu-radiolabeled complexes in selected organs was evaluated at 2, 60, and 240 minutes after tracer administration (Table 5). Excitingly, appreciable brain uptake was observed for all BFCs at 2 min post injection, followed by a rapid washout from the brains of these WT mice (Figure 10). Among all BFCs tested, **^{64}Cu-YW-10** showed the highest brain uptake of 0.46 ± 0.21 %ID/g at 2 min post injection, which dropped to 0.14 ± 0.00 %ID/g at 60 min. **^{64}Cu-YW-7** also exhibits good brain uptake of 0.35 ± 0.01 %ID/g at 2 min post injection (Table 5). The brain to blood ratio results suggest the complex retention in brain slightly increases with time, possibly due to their favorable lipophilicity (Figure 11). The small difference between the esters and acid performance might result from the hydrolysis of the ester groups, generating a stable ^{64}Cu complex with an carboxylic acid arm, that is **^{64}Cu-YW-14**. Overall, these biodistribution studies suggest that the ^{64}Cu-radiolabeled BFCs have moderate brain uptake, and thus could serve as PET imaging agents for detection of Aβ aggregates in vivo. Importantly, the rapid clearance from the brain of WT mice suggest that these radiolabeled BFCs do not release ^{64}Cu ions in the brain to an appreciable extent, and thus should not lead to a significant background PET signal in age-matched WT controls.

Table 5. Overall biodistribution results of ^{64}Cu-labeled **YW-7, YW-8, YW-9, YW-10, and YW-14**, for the three time points evaluated (2, 60, and 240 min; % injected dose per gram, Mean ± SEM).

	YW-7 2 min			**YW-7** 1 h			**YW-7** 4 h			**YW-8** 2 min			**YW-8** 1 h			**YW-8** 4 h		
blood	7.82	±	2.26	0.39	±	0.03	0.16	±	0.03	4.58	±	1.63	0.16	±	0.04	0.07	±	0.01
lung	4.96	±	1.12	1.77	±	0.98	0.76	±	0.18	3.48	±	0.52	0.47	±	0.11	0.34	±	0.04
liver	33.48	±	22.54	5.08	±	1.13	2.56	±	0.67	44.48	±	3.47	4.21	±	2.21	0.83	±	0.13
kidney	10.13	±	6.75	2.81	±	0.76	1.52	±	0.67	9.93	±	1.69	1.42	±	0.44	0.59	±	0.12
muscle	0.75	±	0.40	0.10	±	0.01	0.05	±	0.01	0.84	±	0.06	0.05	±	0.02	0.03	±	0.00
brain	0.35	±	0.01	0.04	±	0.01	0.03	±	0.01	0.23	±	0.06	0.02	±	0.01	0.01	±	0.00
bone	1.18	±	0.36	0.15	±	0.02	0.14	±	0.08	0.98	±	0.05	0.13	±	0.06	0.04	±	0.02
tail	8.84	±	10.15	3.34	±	2.70	2.59	±	3.43	7.33	±	6.22	1.99	±	2.49	0.16	±	0.04

	YW-9 2 min			**YW-9** 1 h			**YW-9** 4 h			**YW-10** 2 min			**YW-10** 1 h			**YW-10** 4 h		
blood	5.08	±	0.79	0.17	±	0.03	0.07	±	0.01	11.57	±	2.40	1.27	±	0.07	0.98	±	0.08
lung	5.05	±	0.55	0.47	±	0.02	0.41	±	0.08	6.87	±	1.62	3.86	±	0.25	5.19	±	0.79
liver	84.61	±	7.49	4.11	±	0.64	0.84	±	0.07	39.82	±	5.59	21.81	±	1.36	15.61	±	2.81
kidney	16.31	±	3.42	1.95	±	0.57	0.60	±	0.08	31.04	±	5.04	14.18	±	3.38	7.49	±	1.54
muscle	1.02	±	0.16	0.06	±	0.00	0.02	±	0.01	1.83	±	0.56	0.56	±	0.16	0.39	±	0.06
brain	0.32	±	0.02	0.02	±	0.00	0.01	±	0.00	0.46	±	0.21	0.14	±	0.00	0.18	±	0.02
bone	1.54	±	0.12	0.10	±	0.02	0.06	±	0.00	2.17	±	0.75	0.75	±	0.03	0.83	±	0.15
tail	3.33	±	0.84	1.00	±	0.27	0.15	±	0.08	4.94	±	4.72	1.57	±	0.06	0.89	±	0.20

	YW-14 2 min			**YW-14** 1 h			**YW-14** 4 h		
blood	5.59	±	0.86	0.10	±	0.04	0.06	±	0.02
lung	4.18	±	0.52	0.21	±	0.03	0.25	±	0.16
liver	51.90	±	2.35	1.74	±	0.49	0.44	±	0.15
kidney	11.74	±	1.16	1.28	±	1.03	0.39	±	0.16

muscle	0.95	±	0.24	0.04	±	0.01	0.03	±	0.02
brain	0.23	±	0.05	0.02	±	0.02	0.02	±	0.00
bone	1.08	±	0.26	0.06	±	0.02	0.06	±	0.02
tail	3.85	±	1.51	5.90	±	5.41	2.60	±	2.11

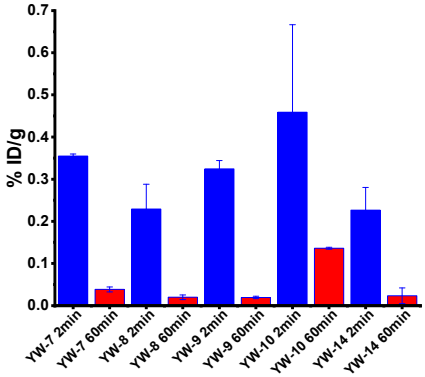

Figure 10. Brain uptake (%ID/g) results from the *in vivo* biodistribution study in CD-1 mice, at 2 and 60 min post injection.

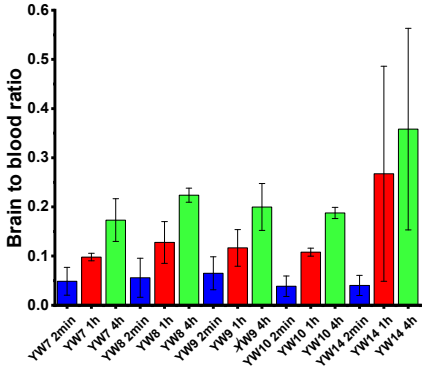

Figure 11. Brain to blood ratio results from the *in vivo* biodistribution study in CD-1 mice, at 2, 60, and 240 min post injection.

CONCLUSIONS

In summary, we have successfully synthesized five BFCs **YW-7** to **YW-14** via linking the amyloid-targeting 2-phenyl benzothiazole fragment with a strong metal chelator TACN, and the resulting BFCs could be radiolabeled with ^{64}Cu for PET imaging purposes. Spectrophotometric titrations were used to obtain stability constants (log K's) for the Cu(II) complexes, and results show that adding a carboxylic acid or ester arm to the TACN fragment increases the log K for the corresponding Cu(II) complexes by 3-4 orders of magnitude vs the parent TACN derivative. Importantly, the BFCs thus exhibit appropriate lipophilicity and Cu-chelating ability to be potentially used in *in vivo* applications. The evaluation of the amyloid binding affinity for these BFCs and their ^{64}Cu complexes was probed by *ex vivo* AD mouse brain section fluorescence imaging and autoradiography studies, which show that the ^{64}Cu complexes of the ester arm BFCs bind more specifically to the amyloid plaques than the ^{64}Cu complex of the carboxylic acid arm BFC, the t-butyl and methyl ester derivatives **YW-7** and **YW-10**, respectively, showing the highest specificity. The ^{64}Cu-radiolabeled BFCs also exhibit favorable *log* D_{oct} values around 1, suggesting they should be BBB permeable. Finally, the *in vivo* biodistribution studies using the ^{64}Cu-BFC complexes reveal that they exhibit moderate brain uptake in CD-1 mice. Overall, we consider that these benzothiazole-TACN BFCs can serve as lead compounds to develop ^{64}Cu PET imaging agents that should benefit in AD diagnosis.

ASSOCIATED CONTENT

Supporting Information. Spectrophotometric titrations, Job's plots, UV-Vis and fluorescence spectra, HPLC chromatograms of radiolabeling assays.

AUTHOR INFORMATION

Corresponding Authors

* mirica@illinois.edu; b.rogers@wustl.edu

Notes

The authors declare no competing financial interest.

ORCID

Liviu Mirica: 0000-0003-0584-9508
Yujue Wang: 0000-0002-5644-5952

ACKNOWLEDGMENTS

This work was supported by the NIH (R01GM114588 to L.M.M.). We thank the small animal imaging facilities at Washington University School of Medicine for excellent technical assistance and the Isotope Production Group at Washington University for the production of ^{64}Cu.

REFERENCES

1. 2020 Alzheimer's disease facts and figures *Alzheimer's & Dementia* **2020**, *16*, 391.
2. DeTure, M. A.; Dickson, D. W. The neuropathological diagnosis of Alzheimer's disease *Mol Neurodegener* **2019**, *14*, 32.
3. Hickey, J. L.; Lim, S.; Hayne, D. J.; Paterson, B. M.; White, J. M.; Villemagne, V. L.; Roselt, P.; Binns, D.; Cullinane, C.; Jeffery, C. M.; Price, R. I.; Barnham, K. J.; Donnelly, P. S. Diagnostic Imaging Agents for Alzheimer's Disease: Copper Radiopharmaceuticals that Target A β Plaques *J. Am. Chem. Soc.* **2013**, *135*, 16120.
4. Tiwari, S.; Atluri, V.; Kaushik, A.; Yndart, A.; Nair, M. Alzheimer's disease: pathogenesis, diagnostics, and therapeutics *Int J Nanomed* **2019**, *14*, 5541.

5. De Strooper, B.; Karran, E. The Cellular Phase of Alzheimer's Disease *Cell* **2016**, *164*, 603.
6. Savelieff, M. G.; Lee, S.; Liu, Y. Z.; Lim, M. H. Untangling Amyloid-beta, Tau, and Metals in Alzheimer's Disease *ACS Chem. Biol.* **2013**, *8*, 856.
7. Nam, G.; Lim, M. H. Intertwined Pathologies of Amyloid-beta and Metal Ions in Alzheimer's Disease: Metal-Amyloid-beta *Chem. Lett.* **2019**, *48*, 951.
8. Cummings, J. L.; Morstorf, T.; Zhong, K. Alzheimer's disease drug-development pipeline: few candidates, frequent failures *Alzheimers Res Ther* **2014**, *6*.
9. Klunk, W. E.; Engler, H.; Nordberg, A.; Wang, Y.; Blomqvist, G.; Holt, D. P.; Bergström, M.; Savitcheva, I.; Huang, G.-F.; Estrada, S.; Ausén, B.; Debnath, M. L.; Barletta, J.; Price, J. C.; Sandell, J.; Lopresti, B. J.; Wall, A.; Koivisto, P.; Antoni, G.; Mathis, C. A.; Långström, B. Imaging Brain Amyloid in Alzheimer's Disease with Pittsburgh Compound-B *Ann. Neurol.* **2004**, *55*, 306.
10. Serdons, K.; Terwinghe, C.; Vermaelen, P.; Van Laere, K.; Kung, H.; Mortelmans, L.; Bormans, G.; Verbruggen, A. Synthesis and evaluation of ^{18}F-labeled 2-phenylbenzothiazoles as positron emission tomography imaging agents for amyloid plaques in Alzheimer's disease *J. Med. Chem.* **2009**, *52*, 1428.
11. Choi, S. R.; Golding, G.; Zhuang, Z.; Zhang, W.; Lim, N.; Hefti, F.; Benedum, T. E.; Kilbourn, M. R.; Skovronsky, D.; Kung, H. F. Preclinical Properties of 18F-AV-45: A PET Agent for Aβ Plaques in the Brain *J. Nucl. Med.* **2009**, *50*, 1887.
12. Choi, S. R.; Golding, G.; Zhuang, Z. P.; Zhang, W.; Lim, N.; Hefti, F.; Benedum, T. E.; Kilbourn, M. R.; Skovronsky, D.; Kung, H. F. Preclinical Properties of F-18-AV-45: A PET Agent for A beta Plaques in the Brain *J. Nucl. Med.* **2009**, *50*, 1887.
13. Uzuegbunam, B. C.; Librizzi, D.; Yousefi, B. H. PET Radiopharmaceuticals for Alzheimer's Disease and Parkinson's Disease Diagnosis, the Current and Future Landscape *Molecules* **2020**, *25*.
14. Sedgwick, A. C.; Brewster, J. T.; Harvey, P.; Iovan, D. A.; Smith, G.; He, X.-P.; Tian, H.; Sessler, J. L.; James, T. D. Metal-based Imaging Agents: Progress towards Interrogating Neurodegenerative Disease *Chem. Soc. Rev.* **2020**, *49*, 2886.
15. Shokeen, M.; Anderson, C. J. Molecular Imaging of Cancer with Copper-64 Radiopharmaceuticals and Positron Emission Tomography (PET) *Acc. Chem. Res.* **2009**, *42*, 832.
16. Wadas, T. J.; Wong, E. H.; Weisman, G. R.; Anderson, C. J. Coordinating Radiometals of Copper, Gallium, Indium, Yttrium, and Zirconium for PET and SPECT Imaging of Disease *Chem. Rev.* **2010**, *110*, 2858.
17. Krasnovskaya, O.; Naumov, A.; Guk, D.; Gorelkin, P.; Erofeev, A.; Beloglazkina, E.; Majouga, A. Copper Coordination Compounds as Biologically Active Agents *Int J Mol Sci* **2020**, *21*.
18. Fodero-Tavoletti, M. T.; Villemagne, V. L.; Paterson, B. M.; White, A. R.; Li, Q. X.; Camakaris, J.; O'Keefe, G. J.; Cappai, R.; Barnham, K. J.; Donnelly, P. S. Bis(thiosemicarbazonato) Cu-64 Complexes for Positron Emission Tomography Imaging of Alzheimer's Disease *J. Alzheimers Dis.* **2010**, *20*, 49.
19. McInnes, L. E.; Noor, A.; Kysenius, K.; Cullinane, C.; Roselt, P.; McLean, C. A.; Chiu, F. C. K.; Powell, A. K.; Crouch, P. J.; White, J. M.; Donnelly, P. S. Potential Diagnostic Imaging of Alzheimer's Disease with Copper-64 Complexes That Bind to Amyloid-beta Plaques *Inorg. Chem.* **2019**, *58*, 3382.
20. Bandara, N.; Sharma, A. K.; Krieger, S.; Schultz, J. W.; Han, B. H.; Rogers, B. E.; Mirica, L. M. Evaluation of ^{64}Cu-based Radiopharmaceuticals That Target Aβ Peptide Aggregates as Diagnostic Tools for Alzheimer's Disease *J. Am. Chem. Soc.* **2017**, *139*, 12550.
21. Sharma, A. K.; Schultz, J. W.; Prior, J. T.; Rath, N. P.; Mirica, L. M. Coordination Chemistry of Bifunctional Chemical Agents Designed for Applications in (64)Cu PET Imaging for Alzheimer's Disease *Inorg. Chem.* **2017**, *56*, 13801.
22. Cho, H. J.; Huynh, T. T.; Rogers, B. E.; Mirica, L. M. Design of a multivalent bifunctional chelator for diagnostic (64)Cu PET imaging in Alzheimer's disease *Proc Natl Acad Sci U S A* **2020**, *117*, 30928.
23. Lim, S.; Paterson, B. M.; Fodero-Tavoletti, M. T.; O'Keefe, G. J.; Cappai, R.; Barnham, K. J.; Villemagne, V. L.; Donnelly, P. S. A copper radiopharmaceutical for diagnostic imaging of Alzheimer's disease: a bis(thiosemicarbazonato)copper(II) complex that binds to amyloid-beta plaques *Chem. Comm.* **2010**, *46*, 5437.
24. Hickey, J. L.; Donnelly, P. S. Diagnostic Imaging of Alzheimer's Disease with Copper and Technetium Complexes *Coord. Chem. Rev.* **2012**, *256*, 2367.
25. Savelieff, M. G.; Nam, G.; Kang, J.; Lee, H. J.; Lee, M.; Lim, M. H. Development of Multifunctional Molecules as Potential Therapeutic Candidates for Alzheimer's Disease, Parkinson's Disease, and Amyotrophic Lateral Sclerosis in the Last Decade *Chem. Rev.* **2019**, *119*, 1221.
26. Huang, Y.; Cho, H.-J.; Bandara, N.; Sun, L.; Tran, D.; Rogers, B. E.; Mirica, L. M. Metal-chelating benzothiazole multifunctional compounds for the modulation and 64Cu PET imaging of Aβ aggregation *Chem. Sci.* **2020**, *11*, 7789.
27. Gomes, L. M. F.; Bataglioli, J. C.; Storr, T. Metal complexes that bind to the amyloid-β peptide of relevance to Alzheimer's disease *Coord. Chem. Rev.* **2020**, *412*, 213255.
28. Joshi, T.; Kubeil, M.; Nsubuga, A.; Singh, G.; Gasser, G.; Stephan, H. Harnessing the Coordination Chemistry of 1,4,7-Triazacyclononane for Biomimicry and Radiopharmaceutical Applications *Chempluschem* **2018**, *83*, 554.
29. De Silva, R. A.; Jain, S.; Lears, K. A.; Chong, H. S.; Kang, C. S.; Sun, X.; Rogers, B. E. Copper-64 radiolabeling and biological evaluation of bifunctional chelators for radiopharmaceutical development *Nucl. Med. Biol.* **2012**, *39*, 1099.
30. Pardridge, W. M. Molecular biology of the blood-brain barrier *Mol. Biotechnol.* **2005**, *30*, 57.
31. Henderson, J. T.; Piquette-Miller, M. Blood-brain barrier: an impediment to neuropharmaceuticals *Clinical pharmacology and therapeutics* **2015**, *97*, 308.
32. Blake, A. J.; Danks, J. P.; Li, W. S.; Lippolis, V.; Schroder, M. Synthesis and characterisation of pendant-arm amino derivatives of 1,4,7-triazacyclononane and alkyl-bridged bis(1,4,7-triazacyclononane) macrocycles and complexation to Cu(II) *J Chem Soc Dalton* **2000**, 3034.
33. Gans, P.; Sabatini, A.; Vacca, A. Determination of equilibrium constants from spectrophotometric data obtained from solutions of known pH: The program pHab. *Ann. Chim.* **1999**, 45.
34. Alderighi, L. Hyperquad simulation and speciation (HySS): A utility program for the investigaion of equilibria involving soluble and partially soluble species. *Coord. Chem. Rev.* **1999**, *184*, 311.
35. Schwetye, K. E.; Cirrito, J. R.; Esparza, T. J.; Mac Donald, C. L.; Holtzman, D. M.; Brody, D. L. Traumatic Brain Injury Reduces Soluble Extracellular Amyloid-β in Mice: A Methodologically Novel Combined Microdialysis-Controlled Cortical Impact Study *Neurobiol. Dis.* **2010**, *40*, 555.
36. Esparza, T. J.; Wildburger, N. C.; Jiang, H.; Gangolli, M.; Cairns, N. J.; Bateman, R. J.; Brody, D. L. Soluble Amyloid-beta Aggregates from Human Alzheimer's Disease Brains *Sci. Rep.* **2016**, *6*, 38187.
37. Kume, M.; Carey, P. C.; Gaehle, G.; Madrid, E.; Voller, T.; Margenau, W.; Welch, M. J.; Lapi, S. E. A Semi-automated System for the Routine Production of Copper-64 *Appl. Radiat. Isot.* **2012**, *70*, 1803.
38. McCarthy, D. W.; Shefer, R. E.; Klinkowstein, R. E.; Bass, L. A.; Margeneau, W. H.; Cutler, C. S.; Anderson, C. J.; Welch, M. J. Efficient Production of High Specific Activity ^{64}Cu using a Biomedical Cyclotron *Nucl. Med. Biol.* **1997**, *24*, 35.
39. See Supporting Information.

40. Biancalana, M.; Koide, S. Molecular mechanism of Thioflavin-T binding to amyloid fibrils *Biochim. Biophys. Acta* **2010**, *1804*, 1405.
41. Mathis, C. A.; Wang, Y.; Holt, D. P.; Huang, G.-F.; Debnath, M. L.; Klunk, W. E. Synthesis and Evaluation of 11C-Labeled 6-Substituted 2-Arylbenzothiazoles as Amyloid Imaging Agents *J. Med. Chem.* **2003**, *46*, 2740.
42. Necula, M.; Kayed, R.; Milton, S.; Glabe, C. G. Small molecule inhibitors of aggregation indicate that amyloid β oligomerization and fibrillization pathways are independent and distinct *J. Biol. Chem.* **2007**, *282*, 10311.
43. Sharma, A. K.; Pavlova, S. T.; Kim, J.; Finkelstein, D.; Hawco, N. J.; Rath, N. P.; Kim, J.; Mirica, L. M. Bifunctional Compounds for Controlling Metal-mediated Aggregation of the A β_{42} Peptide *J. Am. Chem. Soc.* **2012**, *134*, 6625.
44. Lipinski, C. A.; Lombardo, F.; Dominy, B. W.; Feeney, P. J. Experimental and computational approaches to estimate solubility and permeability in drug discovery and development settings *Adv. Drug Delivery Rev.* **2001**, *46*, 3.
45. Perrin, R. J.; Fagan, A. M.; Holtzman, D. M. Multimodal Techniques for Diagnosis and Prognosis of Alzheimer's Disease *Nature* **2009**, *461*, 916.
46. Fagan, A. M.; Holtzman, D. M. Cerebrospinal fluid biomarkers of Alzheimer's disease *Biomark Med* **2010**, *4*, 51.
47. Sun, L.; Sharma, A. K.; Han, B.-H.; Mirica, L. M. Amentoflavone: A Bifunctional Metal Chelator that Controls the Formation of Neurotoxic Soluble A β 42 Oligomers *ACS Chem. Neurosci.* **2020**, *11*, 2741.
48. Storr, T.; Merkel, M.; Song-Zhao, G. X.; Scott, L. E.; Green, D. E.; Bowen, M. L.; Thompson, K. H.; Patrick, B. O.; Schugar, H. J.; Orvig, C. Synthesis, characterization, and metal coordinating ability of multifunctional carbohydrate-containing compounds for Alzheimer's therapy *J. Am. Chem. Soc.* **2007**, *129*, 7453.
49. Choudhary, N.; Jaraquemada-Pelaez, M. D.; Zarschler, K.; Wang, X. Z.; Radchenko, V.; Kubeil, M.; Stephan, H.; Orvig, C. Chelation in One Fell Swoop: Optimizing Ligands for Smaller Radiometal Ions *Inorg. Chem.* **2020**, *59*, 5728.
50. Dischino, D. D.; Welch, M. J.; Kilbourn, M. R.; Raichle, M. E. Relationship between Lipophilicity and Brain Extraction of C-11-Labeled Radiopharmaceuticals *J. Nucl. Med.* **1983**, *24*, 1030.

TOC GRAPHIC

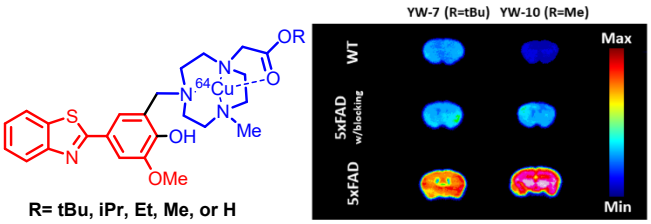
OR
O
N
64Cu
N
N
Me
S
N
OH
OMe
R= tBu, iPr, Et, Me, or H
YW-7 (R=tBu)
YW-10 (R=Me)
WT
5xFAD w/blocking
5xFAD
Max
Min